Coexistence of diffusive and ballistic transport in integrable quantum lattice models

P. Prelovšek,[1,2] M. Mierzejewski [ID],[3] and J. Herbrych [ID][3]

[1]*Jožef Stefan Institute, SI-1000 Ljubljana, Slovenia*
[2]*Faculty of Mathematics and Physics, University of Ljubljana, SI-1000 Ljubljana, Slovenia*
[3]*Department of Theoretical Physics, Faculty of Fundamental Problems of Technology,*
Wrocław University of Science and Technology, 50-370 Wrocław, Poland

We investigate the high-temperature dynamical conductivity $\sigma(\omega)$ in two one-dimensional integrable quantum lattice models: the anisotropic XXZ spin chain and the Hubbard chain. The emphasis is on the metallic regime of both models, where besides the ballistic component, the regular part of conductivity might reveal a diffusivelike transport. To resolve the low-frequency dynamics, we upgrade the microcanonical Lanczos method enabling studies of finite-size systems with up to $L \leqslant 32$ sites for the XXZ spin model with the frequency resolution $\delta\omega \sim 10^{-3}J$. Results for the XXZ chain reveal a fine structure of $\sigma(\omega)$ spectra, which originates from the discontinuous variation of the stiffness, previously found at commensurate values of the anisotropy parameter Δ. Still, we do not find clear evidence for a diffusive component, at least not for commensurate values of Δ, particularly for $\Delta = 0.5$, as well as for $\Delta \to 0$. Similar is the conclusion for the Hubbard model away from half-filling, where the spectra reveal more universal behavior.

I. INTRODUCTION

One of the basic features of the integrable quantum many-body lattice is the possibility of the ballistic/dissipationless transport at finite temperatures (for a recent review see [1]). This property, which is manifested in a finite value of corresponding transport stiffnesses $D > 0$, has been well established in the most investigated one-dimensional (1D) integrable model, the anisotropic XXZ spin chain within the easy-plane regime with the anisotropy $\Delta < 1$, but also in the 1D Hubbard model away from half-filling. Finite stiffness $D > 0$ has been resolved via the sensitivity of levels to the imposed magnetic flux [2], using the thermodynamic Bethe ansatz (TBA) [3–6], and with more rigorous bounds via the Mazur inequality [7] which relate D to the overlap with local and quasilocal conserved quantities [8–11]. The latter result agree also with a more general approach via the generalized hydrodynamics (GHD) [12–14]. Furthermore, results for $D > 0$ and ballistic transport have been confirmed in numerous numerical studies of finite XXZ chains [15–26]. In spite of these advances there remains an open question whether analytical theories also quantitatively fix values of D, in particular its dependence on the anisotropy Δ within the XXZ chain in the high-T regime [9,14,23,25,27–29] (see the discussion in [1]).

Much less attention has been devoted to the whole dynamical response, as represented by the real part of the frequency-dependent conductivity at $T > 0$,

$$\sigma(\omega) = 2\pi D \delta(\omega) + \sigma_{\text{reg}}(\omega), \tag{1}$$

which can be (in a metallic regime of considered models) decomposed into the ballistic $D > 0$ component and the regular (incoherent) part $\sigma_{\text{reg}}(\omega)$. Exact-diagonalization (ED) results on finite-size XXZ chains [15,22], as well as on the particular case of the Hubbard chain [16], indicate on vanishing (dc) limit, $\sigma_{\text{reg}}^0 = \sigma_{\text{reg}}(\omega \to 0) \to 0$, consistent with the argument based on the level crossing in integrable lattice models [30] implying $\sigma_{\text{reg}}(\omega \to 0) \propto \omega^2$, at least for finite-size systems. Less conclusive are results obtained via a time-dependent density-matrix renormalization group (tDMRG) method on a larger system but with restricted time evolution (or equivalently with limited frequency resolution), allowing for $\sigma_{\text{reg}}^0 > 0$ [25,26]. The latter can be interpreted as coexistence of ballistic transport and (subleading) diffusion response. This question is challenging since some analytical approaches [31,32], and in particular more recently the GHD approach [33–37], generally predict besides $D > 0$ also $\sigma_{\text{reg}}^0 > 0$. That is, within the XXZ chain the GHD yields finite values of $\sigma_{\text{reg}}^0 > 0$ at the commensurate values $\Delta_m = \cos(\pi/m)$ and, moreover, singular $\sigma_{\text{reg}}(\omega \to 0) \propto \omega^{-\alpha}, \alpha > 0$ [36,37] behavior.

To comment on the dynamical transport $\sigma(\omega)$, at least from the perspective of the linear response in finite-size systems with periodic boundary conditions (PBC), we perform the numerical calculation of high-T limit of $\tilde{\sigma}(\omega) = T\sigma(\omega)$ in the XXZ model, scanning the whole range of anisotropies $\Delta < 1$, but also in the Hubbard chain away from half-filling. Note that both models exhibit the finite stiffness $\mathcal{D} = TD > 0$ for the considered model parameters. To resolve the low-ω regime, we employ, besides ED for smaller systems, the upgraded microcanonical Lanczos method (MCLM) [38] with the high-ω resolution, i.e., for the XXZ chain of length $L \leqslant 32$ we reach $\delta\omega \sim 10^{-3}J$ (equivalent to time evolution up to
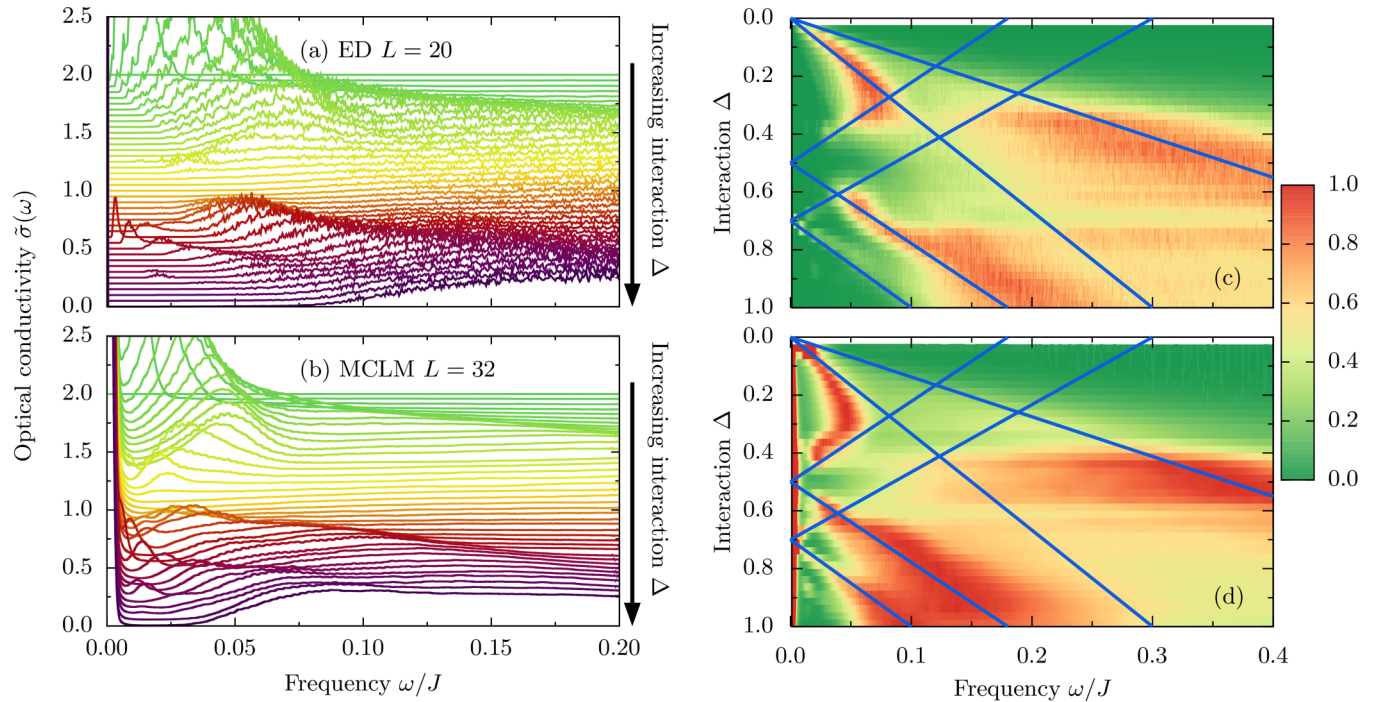
FIG. 1. High-T spin conductivity $\tilde{\sigma}(\omega) = T\sigma_{\mathrm{reg}}(\omega)$ in the XXZ spin chain for the anisotropy range $\Delta \leqslant 1$ ($\Delta = 0, 0.025, \ldots, 1.0$), as calculated by (a) ED for $L = 20$ sites and (b) MCLM for $L = 32$ sites. Each consecutive curve is given an offset for better visibility. (c) and (d) Heat maps of results from (a) and (b), respectively. For clarity, the latter results are normalized by a maximum of $\tilde{\sigma}_{\mathrm{reg}}(\omega)$. Guidelines on both panels mark the positions of the low-frequency peaks obtained for $L = 20$.

$\tau \sim 5 \times 10^3/J$). Such a resolution allows us to disentangle, according to Eq. (1), well enough the dissipationless part from the low-$\omega \tilde{\sigma}_{\mathrm{reg}}(\omega)$.

In Fig. 1 we present one of the main results of our findings (discussed in Sec. II C in more detail), i.e., changing the value of anisotropy Δ reveals a quite complicated fine structure of $\tilde{\sigma}_{\mathrm{reg}}(\omega)$ spectra, here presented as the result of full ED for the $L = 20$ system, as well as for the $L = 32$ chain evaluated with MCLM. The structure can be traced back to discontinuities (or at least anomalies) of $\mathcal{D}$ found at commensurate $\Delta = \Delta_m$ [1] (even in finite systems). The spectral weight related with the discontinuities $\mathcal{D}(\Delta_m) - \lim_{\Delta \to \Delta_m} \mathcal{D}(\Delta)$ is transferred to low-frequency peaks of $\tilde{\sigma}_{\mathrm{reg}}(\omega)$ centered at $\omega_p \propto |\Delta - \Delta_m|$. Still, we do not find a clear evidence (or at least a very small upper bound) for $\tilde{\sigma}_{\mathrm{reg}}^0$ at commensurate $\Delta_m = \cos(\pi/m)$, in particular for $\Delta = \Delta_3 = 0.5$. In order to identify the positions of peaks at ω_p, in Figs. 1(c) and 1(d) we plot $\tilde{\sigma}_{\mathrm{reg}}(\omega)/\tilde{\sigma}_{\mathrm{max}}$, where $\tilde{\sigma}_{\mathrm{max}}$ is the maximum of $\tilde{\sigma}_{\mathrm{reg}}(\omega)$. The lines mark the positions of ω_p determined from $L = 20$ ED data [Fig. 1(c)] and are put also on top of $L = 32$ MCLM data [Fig. 1(d)]. Here the main message is that generally ω_p weakly depends on L, whereby the exceptions are the regime of $\Delta \to 1$, but also at $0.1 < \Delta < 0.5$ where we notice possibly significant reduction of ω_p with L. In order to properly resolve the latter regime $\Delta \to 0$, we apply also the degenerate-perturbation-theory (DPT) method [29]. Results confirm a pronounced peak in $\tilde{\sigma}_{\mathrm{reg}}(\omega \sim \omega_p)$ with $\omega_p \propto \Delta$ and $\tilde{\sigma}_{\mathrm{reg}}(\omega \ll \omega_p) \sim \omega^2$. Furthermore, results for the 1D Hubbard model obtained at generic quarter-filling $\bar{n} = 1/2$ also reveal—besides more universal structure of dynamical charge conductivity $\tilde{\sigma}_c(\omega)$—no clear indication for finite diffusion component $\tilde{\sigma}_{c,\mathrm{reg}}^0$.

II. SPIN CONDUCTIVITY IN THE XXZ CHAIN

We consider in more detail a 1D anisotropic XXZ spin model,

$$H = \frac{J}{2} \sum_i (e^{i\phi} S_{i+1}^+ S_i^- + \mathrm{H.c.}) + J\Delta \sum_i S_{i+1}^z S_i^z, \quad (2)$$

on a chain with length L and with generalized PBC. Here S_i^α with $\alpha = +, -, z$ represent the standard $S = 1/2$ operators. We focus on the metallic regime with the anisotropy parameter $0 < \Delta < 1$, revealing the $T > 0$ dissipationless transport with $D > 0$. We further evaluate only canonical systems with zero magnetization, i.e., $S_{\mathrm{tot}}^z = 0$. At fixed L and at PBC, the results might depend on the phase shift ϕ. Since in the following we numerically study systems $L = 4\mathcal{L}$, i.e., $L = 16, 20, \ldots, 32$, we choose $\phi = \pi/L$ (equivalent to anti-PBC) in order to stay consistent with our previous studies of the fermionic version of the model, i.e., the t-V model [15,29]. Note that considered systems at $S_{\mathrm{tot}}^z = 0$ have an even number of fermions. We further use $\hbar = k_B = 1$ as well as fix $J = 1$ as the unit of energy.

We concentrate on high-T dynamical spin conductivity $\tilde{\sigma}(\omega) = T\sigma(\omega)$, within the linear response theory for $T \gg J$ given by

$$\tilde{\sigma}(\omega) = \frac{\pi}{LN_{\mathrm{st}}} \sum_{n,m} |\langle n|j|m\rangle|^2 \delta(\omega - \epsilon_m + \epsilon_n), \quad (3)$$

expressed here in terms of many-body (MB) eigenstates $|n\rangle$ and eigenvalues ϵ_n, with the spin current $j = (J/2) \sum_i (ie^{i\phi} S_{i+1}^+ S_i^- + \mathrm{H.c.})$, and N_{st} as the total number of MB states for given L and S_{tot}^z. Besides $S_{\mathrm{tot}}^z = 0$ we use also

translational symmetry of the model [Eq. (2)] so that calculation of Eq. (3) is performed as the sum over all wave-vector-q sectors.

A. Numerical method

For smaller systems $L \leqslant 20$ (for the XXZ model) we evaluate Eq. (3) directly via the full ED finding all $|n\rangle$, ϵ_n. For larger L we employ the MCLM [38,39], used in several studies of dynamical transport in (mostly disordered) spin systems [40]. Since the aim in the present problem is to achieve besides large L (with the Hilbert space up to $N_{st} \sim 10^8$) also well resolved spectra at $\omega \sim 0$, we upgrade MCLM by enabling very high frequency resolution $\delta\omega \sim 10^{-3}J$. The calculation steps are the following: (a) The sum over eigenstates in Eq. (3) is replaced with the microcanonical state $|\Psi_{\mathcal{E}}\rangle$ corresponding to the energy $\mathcal{E}$. The latter is obtained with $M_L \gg 1$ Lanczos steps using the operator $V = (H - \mathcal{E})^2$. For larger systems, such a procedure is not expected to converge to exact eigenvalues of H, but rather to a wave function with a small energy dispersion $\sigma_{\mathcal{E}}^2 = \langle\Psi_{\mathcal{E}}|V|\Psi_{\mathcal{E}}\rangle$. By performing Lanczos procedure twice and by extracting lowest eigenfunction only, we avoid the full diagonalization of the $M_L \times M_L$ matrix. (b) In the second step, $\tilde{\sigma}(\omega)$ is evaluated as the resolvent

$$\tilde{\sigma}(\omega) = \frac{1}{L}\text{Im}\langle\Psi_{\mathcal{E}}|j\frac{i}{\omega + i\eta + \mathcal{E} - H}j|\Psi_{\mathcal{E}}\rangle, \quad (4)$$

evaluated again with M_L Lanczos steps starting with initial wave function $j|\Psi_{\mathcal{E}}\rangle$. Finally, Eq. (4) is expressed in terms of continued fractions and is evaluated for small η. M_L determines the frequency resolution as $\delta\omega \sim \Delta E/M_L$, where ΔE is the energy span of H for fixed L. Since for given M_L we have $\sigma_{\mathcal{E}} < \delta\omega \sim \eta$, one can directly choose desired $\delta\omega$ by increasing M_L, even well beyond $M_L \sim 10^4$. To reduce statistical error, we use besides translational symmetry (with $M_q = L$ different q) also additional sampling over $M_s \geqslant 1$ targeted energies $\mathcal{E}_{qs}$ with a Gaussian distribution corresponding to a high-T value of $\langle H^2\rangle \sim L/8$ for given L. The final result is the average $\tilde{\sigma}(\omega) = 1/(M_q M_s)\sum_{qs}\tilde{\sigma}(\mathcal{E}_{qs}, \omega)$.

In the present application to the XXZ chain, we choose $M_L = 2 \times 10^4$, $M_s = 4$ for the $L = 28$ system and $M_L = 10^4$, $M_s = 1$ for the $L = 32$ chain which has $N_{st} \sim 2 \times 10^7$ in a given symmetry sector with fixed q and S_{tot}^z. It is worth noting that that our method is related to dynamical-quantum-typicality (DQT) approach to time-dependent correlation functions at $T \gg 0$ [24]. The latter method employs the evolution in the time domain, whereby our results would imply reaching times up to $\tau \sim 2\pi/\delta\omega > 5 \times 10^3/J$ for considered systems.

To capture $\tilde{\sigma}(\omega)$ spectra including the singular $\mathcal{D} > 0$ component, it is convenient to present the integrated intensity $I(\omega) = (2T/\pi)\int_0^\omega \sigma(\omega')d\omega'$. Here we note that $I(\omega \to 0) = 2\mathcal{D}$, while the sum rule at $S_{tot}^z = 0$ gives $I_\infty = I(\omega \to \infty) = \langle j^2\rangle/L = (1/8)[1 + 1/(L-1)]$ including a small $1/L$ correction. To reveal the feasibility of the MCLM, in Fig. 2 we present the renormalized $\tilde{I}(\omega) = I(\omega)/I_\infty$ as obtained for different sizes $L = 16$–32 (whereby $L = 16, 20$ results are obtained via full ED) for three characteristic $\Delta = 0.2, 0.6, 1.0$. Results are presented in log-ω scale in order to amplify the low-ω regime at $\omega > 2 \times 10^{-3}$, beyond the $\mathcal{D} > 0$ contribu-
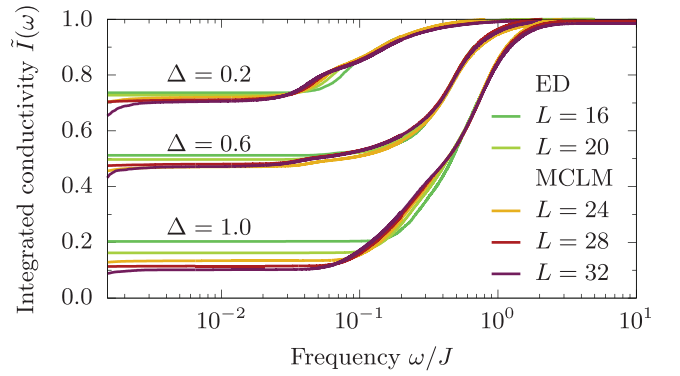

FIG. 2. Integrated and normalized dynamical spin conductivity $\tilde{I}(\omega) = I(\omega)/I_\infty$ in a log-ω scale within the XXZ spin chain for selected $\Delta = 0.2, 0.6, 1.0$, as calculated for different sizes, i.e., $L = 16, 20$ using full ED, and $L = 24, 28, 32$ using MCLM.

tion, in MCLM smeared within $\omega < \delta\omega$. It should be stressed that the MCLM method calculates the whole dynamical response $\tilde{\sigma}(\omega)$, so it is essential to have high $\delta\omega$ resolution in order to well separate the singular $\mathcal{D} > 0$ (restricted to $\omega < \delta\omega$) contribution from the regular part $\tilde{\sigma}_{reg}(\omega)$. On the other hand, the separation of regular and singular part is facilitated since we find for all considered (finite-size $L \leqslant 32$) systems $\tilde{\sigma}_{reg}(\omega \to 0) \sim 0$. This separation is additionally tested via comparison to the ED results, where the ballistic component is obtained directly from diagonal matrix elements in Eq. (3).

Presented results reveal generally quite small $\tilde{\sigma}_{reg}(\omega)$ at low-$\omega < 0.02$ for presented $\Delta \lesssim 0.6$ and for all L. Still, ω dependence is quite pronounced in the intermediate frequency regime, depending crucially on Δ. On the other hand, on approaching the isotropic case $\Delta \to 1$, the results in Fig. 2 confirm pronounced L dependence of the dissipationless component $I(\omega \to 0) = 2\mathcal{D}$. The latter is expected to vanish for $L \to \infty$ [41] for $\Delta = 1$, while the regular part should approach the superdiffusive transport [34,42–45].

B. Commensurate anisotropies Δ_m

Let us first focus on results for the commensurate values of the anisotropy $\Delta_m = \cos(\pi/m)$ and on the possibility of the coexistence of ballistic component $\mathcal{D} > 0$ and finite diffusion, i.e., $\tilde{\sigma}_{reg}^0 > 0$. Since L dependence might be important, in Fig. 3 we present results obtained for different $L = 20$–32 for two specific commensurate points $m = 3$ ($\Delta_3 = 0.5$) and $m = 4$ ($\Delta_4 = 1/\sqrt{2} \simeq 0.707$). The most clear case appears to be $\Delta = 0.5$, where taking into account finite smearing due to $\delta\omega$, it is hard to claim finite $\tilde{\sigma}_{reg}^0 > 0$. Results are more consistent with the presence of a soft gap for $\omega < \omega_g$. The gap may be roughly estimated from the change of slope of $\tilde{\sigma}_{reg}(\omega)$. In particular, for $\Delta = \Delta_3$ and $L = 32$ such change of slope is well visible in Fig. 3(a) at $\omega_g \simeq 0.08$. The regular part appears to vanish inside the gap as $\tilde{\sigma}_{reg}(\omega < \omega_g) \propto \omega^\zeta$ with $\zeta > 1$ as shown in the inset in Fig. 3. However, ω_g reveals some L dependence which could be possibly made compatible even with its vanishing in the thermodynamic limit. At least we can put some upper bound on $\tilde{\sigma}_{reg}^0$. Given that the optical conductivity increases with the frequency for $0 < \omega < 0.4$ and that $\tilde{\sigma}_{reg}(\omega > 0.15)$ shows no finite-size effects, we estimate
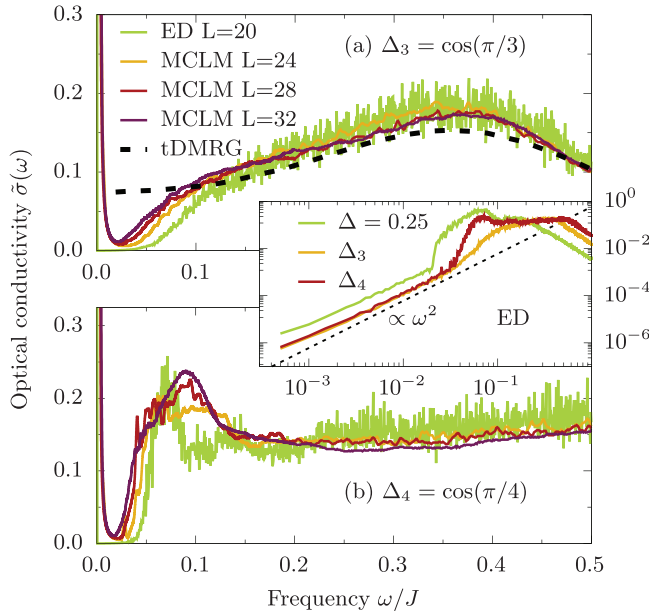
FIG. 3. Spin conductivity $\tilde{\sigma}(\omega)$ obtained for different $L = 20$–32 for two commensurate $\Delta = \cos(\pi/m)$: (a) $m = 3$ ($\Delta = 0.5$), where the dotted line is the result of tDMRG [25], and (b) $m = 4$, $\Delta = 1/\sqrt{2} \simeq 0.707$. Inset shows $\tilde{\sigma}_{\text{reg}}(\omega)$ (using logarithmic scale) obtained from ED for selected values of Δ together with a guideline $\sim \omega^2$.

$\tilde{\sigma}_{\text{reg}}^0 < \sigma_{\text{reg}}(\omega = 0.15) < 0.1$. This bound can be compared with the value $\tilde{\sigma}_{\text{reg}}^0 \sim 0.0685$ obtained by the GHD approach [33,36]. In Fig. 3(a) we plot also the result obtained with tDMRG on a much bigger system [25], but with a restricted time span $\tau < 35/J$. The agreement for larger $\omega > 0.1$ is quite satisfactory indicating less relevant L dependence in this regime. On the other hand, the deviation for $\omega < 0.1$ is not surprising since (referring to the authors of [25]) the spectra for $\omega < 0.15$ are beyond the reach of their study.

Our results for Δ_4 are somewhat less conclusive due to quite a pronounced low-ω peak at $\omega \sim 0.1$ which, however, does not shift significantly with L (in contrast to the case $\Delta \to 1$ as presented in Fig. 2). We should also point out that when speculating on possible closing of the (again soft) spectral gap in Fig. 3(a) or 3(b) for both Δ_m with $L \to \infty$, this should be done by keeping moments $\mu_n = \int_0^\infty \omega^n \tilde{\sigma}(\omega) d\omega$ unchanged, since they are correctly reproduced in finite systems (as well as in MCLM) up to to high order $n = L$. In any case, our results for $m = 4$ should be compared with the GHD result $\tilde{\sigma}_{\text{reg}}^0 \sim 0.14$ (see Supplemental Material of Ref. [33]).

C. General structure of $\tilde{\sigma}(\omega)$

To discuss the structure of $\tilde{\sigma}(\omega)$ in the whole regime $\Delta < 1$, we first present in Fig. 4 the evolution of $I(\omega)$ with Δ as obtained via MCLM on $L = 32$ system with the resolution $\delta\omega \sim 10^{-3}$. The advantage of $I(\omega)$ is that it yields direct information on the stiffness $2\mathcal{D} = I(\omega \to 0)$ discussed before [1,29]). Results indicate that in the regime $\Delta \lesssim 0.5$ the major part of the $I(\omega)$ response is in the dissipationless component $\mathcal{D}$. Moreover, our results for $\mathcal{D}$ are in this regime quantitatively consistent with previous DQT analysis [23,24] and with
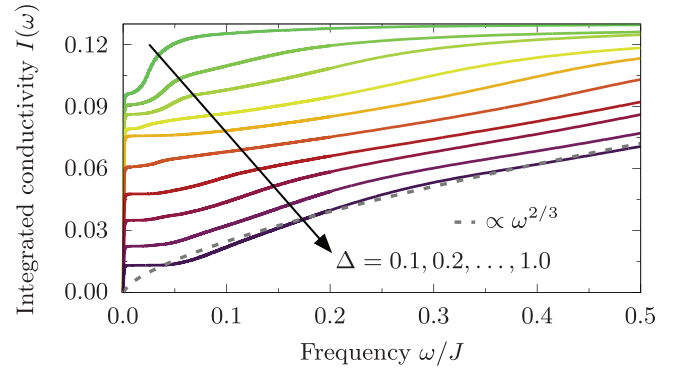

FIG. 4. Integrated spin conductivity $I(\omega)$ for the whole range of $\Delta = 0.1$–1.0, as obtained via MCLM on $L = 32$ XXZ spin chain. For $\Delta = 1$ we show also the fit for superdiffusive $I(\omega) \propto \omega^{2/3}$.

the DPT method for $\Delta \to 0$ [29], which both yield a value significantly above the one representing the lower-bound/GHD result [1,9,37]. For $\Delta \gtrsim 0.5$ the major part in $I(\omega)$ is in the regular response and the mismatch with GHD lower bound is less evident. It follows from Fig. 2 that ED/MCLM results for $\Delta \to 1$ exhibit considerable L dependence showing up in the apparent $\mathcal{D} > 0$, but also in closing of the finite-size gap (being $\omega_g \sim 0.05$ for $L = 32$). It is, however, well visible that for $\omega > \omega_g$ at $\Delta = 1$ the spectra in Fig. 4 can be well fitted with $I(\omega) \propto \omega^{2/3}$ implying the superdiffusive response $\tilde{\sigma}(\omega) \propto \omega^{-1/3}$ [34,36,37,42–45].

Beyond dissipationless $\mathcal{D} > 0$ component, $I(\omega)$ in Fig. 4 reveals a quite complex evolution of $\tilde{\sigma}_{\text{reg}}(\omega)$ with Δ, in particular for $\Delta > 0.2$ there are visible more than one inflexion point with $d^2I(\omega)/d\omega^2 = 0$ corresponding to peaks in $\tilde{\sigma}_{\text{reg}}(\omega)$. Moreover, direct information on $\tilde{\sigma}_{\text{reg}}(\omega)$ is presented in Fig. 1 (obtained on $L = 20$ via ED and $L = 32$ via MCLM). Note that in the latter case, at $\omega < \delta\omega \sim 10^{-3}$, the spectra are dominated by the singular (but broadened) dissipationless component $\mathcal{D} > 0$. Nevertheless, the structure of peaks consistent with Fig. 1(a) is still visible in Fig. 1(b). As discussed recently [29], at small $\Delta < 0.2$ a single peak at $\omega_p \propto \Delta$ dominates $\tilde{\sigma}_{\text{reg}}(\omega)$ and is analyzed in Sec. II D in more detail.

In the intermediate regime $0.2 \lesssim \Delta < 0.5$ the structure of $\sigma_{\text{reg}}(\omega)$ evolves into two peaks, i.e., the upper part still with $\omega_{p1} \propto \Delta$ retaining most of the sum rule of $\sigma_{\text{reg}}(\omega)$, while the lower peak ω_{p2} splits off and is expected to vanish at commensurate $\Delta_3 = 0.5$ as $\omega_{p2} \propto |\Delta_3 - \Delta|$. Such evolution is consistent with the specific behavior at commensurate points, $\Delta_m = \cos(\pi/m)$ [3,8,9], where also additional degeneracies (diagonal as well as off-diagonal in S_{tot}^z [29,46]) exist. The latter macroscopic degeneracies of the energy spectrum should coincide with discontinuous variation (jumps) of the stiffness $\mathcal{D}$ at these particular values $\Delta = \Delta_m$. At the same time, the frequency moments μ_n (up to large $n \sim L$) are continuous functions of Δ, even close to commensurate values. The simplest scenario which may capture both features is that the missing spectral weight $\mathcal{D}(\Delta_m) - \lim_{\Delta \to \Delta_m} \mathcal{D}(\Delta)$ is transferred to narrow low-frequency peaks centered at frequencies $\omega_{pm} \propto |\Delta_{m+1} - \Delta|$. In particular, we can confirm such a scenario by our detailed numerical analysis (ED for $L = 20$)
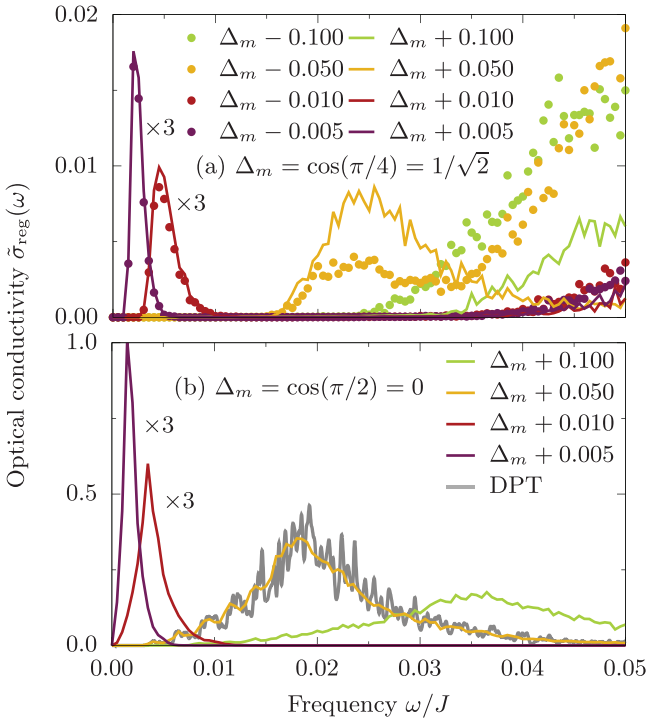
FIG. 5. Detailed analysis of $\tilde{\sigma}_{\mathrm{reg}}(\omega)$ spectra in the vicinity of (a) $\Delta_4 = 1/\sqrt{2}$ and (b) $\Delta_2 = 0$ anisotropy, as calculated for $L = 20$ sites by ED. The DPT result is also marked in (b).

for the vicinity of $\Delta_4 = 1/\sqrt{2}$, as presented in Fig. 5(a). It clearly shows the emergence of symmetric peaks at $\Delta \sim \Delta_4$. At the same time, also the widths of these peaks appear to scale as $\delta\omega_{pm} \propto |\Delta_{m+1} - \Delta|$. Both these facts show qualitative analogy to the situation close to $\Delta = \Delta_2 = 0$, presented in Fig. 5(b), where the development with a single peak at the frequency $\omega_p \propto \Delta$ can be followed much more in detail [29] (see also more elaborate analysis and discussion in Sec. II D). It should be, however, noted that in a finite system one can follow a jump in $\mathcal{D}$ and the related emergence of peaks in $\tilde{\sigma}_{\mathrm{reg}}(\omega)$ only provided that the particular MB states at a given L and S^z_{tot} display a large degeneracy at commensurate Δ_m. This is indeed the case for Δ_2 and Δ_4 assuming the considered here finite systems $L = 4\mathcal{L}$. On the other hand, at $\Delta_3 = 0.5$ our systems do not reveal explicit (large) degeneracy, so the above phenomena cannot be followed in the very vicinity of Δ_3, but they become more evident with the increasing system size as in Figs. 1(b) and 1(d) for $L = 32$.

The above scenario should imply also for $\Delta > \Delta_3 = 0.707$ further peaks emerging and leading to quite complex low-ω structure of $\tilde{\sigma}_{\mathrm{reg}}(\omega)$ on approaching $\Delta \to 1$. However, results for $\Delta > 0.8$ should be taken with some reservation, since they already reveal significant L dependence. In particular, at $\Delta \to 1$ one expects the vanishing coherent part $\mathcal{D} \to 0$, while the observed spectral gap $\omega_g \propto 1/L^\zeta$, well visible in Fig. 1, below quite featureless spectra is known to be a finite-size effect [41]. This gap reflects the anomalous L dependence of $\tilde{\sigma}_{\mathrm{reg}}(\omega)$ in the integrable XXZ chain in the insulating regime $\Delta > 1$ [21] and, in particular, the superdiffusion at $\Delta = 1$ [34,42–45], discussed in connection with Fig. 4.

D. The case of small $\Delta \ll 0.5$

Results for $L = 20$ and $L = 32$ shown in Figs. 1(c) and 1(d) demonstrate that the position of the single peak at ω_p strongly depends on L only for $\Delta < 0.5$. In this subsection we carry out the finite-size scaling of $\sigma_{\mathrm{reg}}(\omega \to 0)$ in the regime of small Δ. At $\Delta = 0$, the current operator commutes with the Hamiltonian, thus $\tilde{\sigma}(\omega) = 2\pi \mathcal{D} \delta(\omega)$ and the regular part is absent. There is also a large jump (discontinuity) of the stiffness at $\Delta \to 0$ [1,29]. Similarly to other commensurate points, the spectral weight $\mathcal{D}(0) - \lim_{\Delta \to 0} \mathcal{D}(\Delta)$ is transferred to $\omega > 0$ for $\Delta \neq 0$. The latter weight forms a peak at $\omega_p \propto \Delta$, see Figs. 1 and 5(b). As a consequence, the regime of weak interaction is unique in that the structure of $\tilde{\sigma}(\omega)$ is relatively simple.

To evaluate $\tilde{\sigma}(\omega)$, we employ a recent approach which targets the regime of $\Delta \ll 0.5$. For details we refer to [29], where the focus was on the stiffness $\mathcal{D}$, which requires calculation of the diagonal matrix elements $\langle n|j|n\rangle$ for $\Delta \neq 0$. The eigenstates $|n\rangle$ can be obtained via the DPT starting from the noninteracting case $\Delta = 0$, with a highly degenerate energy spectrum. The value of $\mathcal{D}$ obtained from the latter approach agrees with the ED results up to the numerical precision [29]. We extend these calculations to obtain also the off-diagonal matrix elements $\langle n|j|m\rangle$ and the corresponding $\tilde{\sigma}_{\mathrm{reg}}(\omega)$ defined in Eq. (3). In Fig. 5(b) we compare the DPT and ED results for $L = 20$ sites and find perfect agreement. Note, however, that the DPT does not require any ω smoothing, i.e., it has full frequency resolution, and allows for full analysis of large system sizes, i.e., up to $L = 28$.

Figure 6(a) shows the integrated regular part $I_{\mathrm{reg}}(\omega)$ for (arbitrarily chosen small) $\Delta = 0.1$ and various system sizes L. For convenience, the presented quantity is normalized so that $I_{\mathrm{reg}}(\omega \to \infty) = 1$. Since we apply the perturbative approach, the very same results hold true for arbitrary $\Delta \ll 0.5$, up to rescaling of frequency $\omega \to \omega \Delta/0.1$. In order to estimate the $\tilde{\sigma}_{\mathrm{reg}}(\omega \to 0)$ in the $L \to \infty$ limit, we first note the power-law dependence of the low-ω part $I_{\mathrm{reg}}(\omega \ll \omega_p) \propto \omega^{b+1}$ so that $\tilde{\sigma}_{\mathrm{reg}}(\omega) \propto \omega^b$. The power-law fits are shown as straight lines in Fig. 6(b) and the resulting exponents b are plotted in Fig. 6(d) as a function of $1/L$. The latter function shows a positive curvature, thus a straight (continuous, green) line going through the results for two largest L may serve as a lower bound for b. These results indicate that $1 \leqslant b \leqslant 2$ for $L \to \infty$ with the possibility of the analytic form $\tilde{\sigma}_{\mathrm{reg}}(\omega \ll \omega_p) \propto \omega^2$ [30]. Figure 6(c) shows the asymptotic behavior of $1 - I_{\mathrm{reg}}(\omega)$, where one observes that the response decays exponentially for $\omega \gg \omega_p$. Finally, we estimate the L dependence of ω_p, which corresponds to the position of largest slope in Fig. 6(a), and is shown in Fig. 6(d). For comparison we show also the median value ω_m defined as $I_{\mathrm{reg}}(\omega_m) = 0.5$. Both quantities apparently follow linear dependence in $1/L$. The extrapolation (which within DPT represents more a lower bound) of this trend suggests that in the thermodynamic limit $\omega_m > 0$ and $\omega_p > 0$. Since DPT results in Fig. 6(d) suggest that $\omega_m \sim \omega_p$ for all L, we present in the inset of Fig. 6(a) also the rescaled quantity $I_{\mathrm{reg}}(\omega/\omega_p)$, which indeed appears to be quite universal for all L. Still, this is only approximately true, since also exponent b changes (slightly) with L, as summarized also in Figs. 6(b) and 6(d).
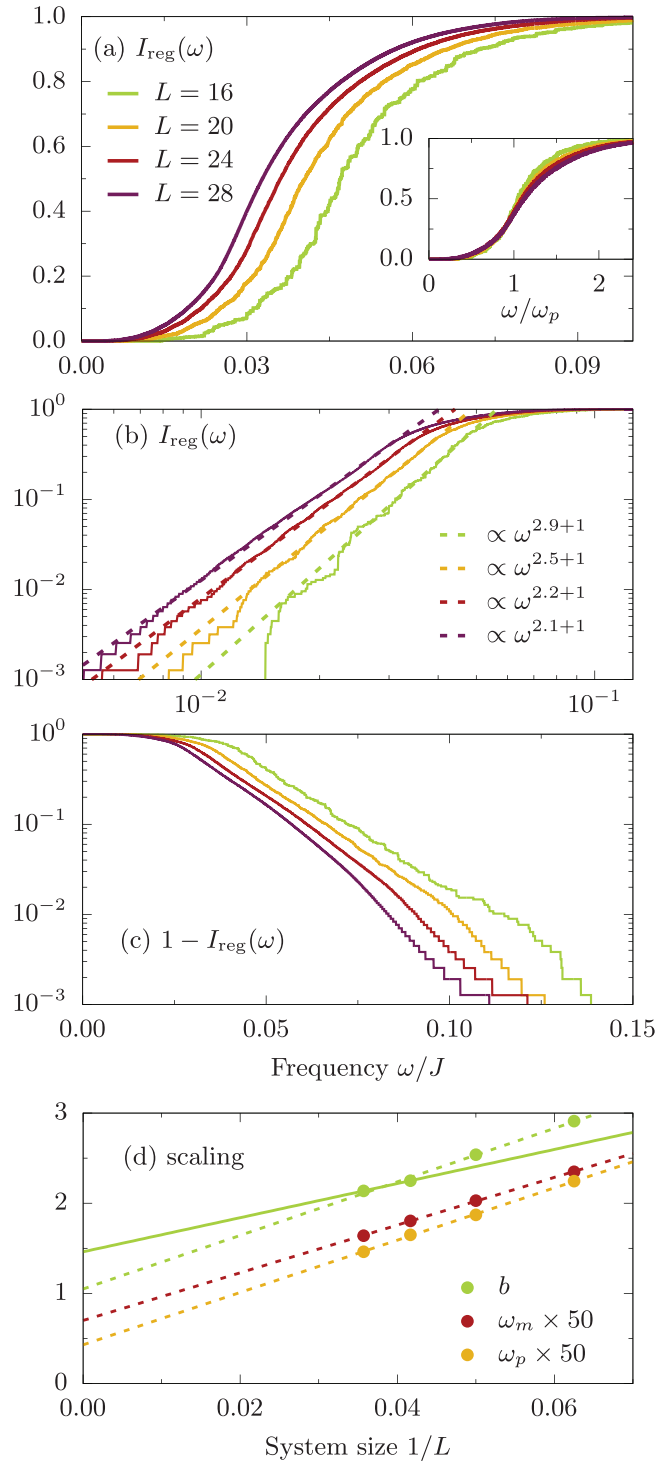
FIG. 6. (a) Integrated and normalized regular part of the optical conductivity $I_{reg}(\omega)$ obtained for $L = 16$–28 sites via the DPT calculation for $\Delta \to 0$. The inset shows rescaled data $I_{reg}(\omega/\omega_p)$, where ω_p is the position of maximum. (b) The low-frequency part of $I_{reg}(\omega \ll \Delta)$ fitted by $I_{reg} \propto \omega^{b+1}$ (fits are shown as dashed lines). (c) Exponential decay of $1 - I_{reg}(\omega)$. (d) Finite-size scaling of the exponent b from (b), where the dashed line shows fits linear in $1/L$ and the continuous guideline goes through results for $L = 24$ and $L = 28$. In (d) we present also the position of peak ω_p and median ω_m together with the linear fits.

III. 1D HUBBARD MODEL

Another relevant model for the possible coexistence of ballistic and diffusive transport is the integrable 1D Hubbard model of interacting fermions,

$$H = -t \sum_{is} (c^{\dagger}_{i+1,s} c_{i,s} + \text{H.c.}) + U \sum_{i} n_{i\uparrow} n_{i\downarrow}, \quad (5)$$

again on a chain of length L with PBC, where we consider states with fixed number $N_{\uparrow}, N_{\downarrow}$ of up- and down-spin fermions, respectively. The properties of the model depend on the filling (density) $\bar{n} = (N_{\uparrow} + N_{\downarrow})/L$ and the magnetization $\bar{m} = (N_{\uparrow} - N_{\downarrow})/L$. Here one can define both charge j_c and spin j_s currents, so we can discuss corresponding conductivities as well as stiffnesses $\mathcal{D}_c, \mathcal{D}_s$, respectively. Most recent studies of the 1D Hubbard model focused on the half-filling case, i.e., $\bar{n} = 1$ and $\bar{m} = 0$ [1,12,13,26], where both stiffnesses vanish, i.e., $\mathcal{D}_c = \mathcal{D}_s = 0$, due to the relation with the isotropic Heisenberg model. This is not the case for $\bar{n} \neq 1$ [13], where $\mathcal{D}_c$ and $\mathcal{D}_s$ also exhibit in general a jump in the proximity to the noninteracting limit $U \to 0$ [29] (in analogy to the $\Delta \to 0$ in the XXZ model). It should be also reminded that the first example of the ballistic transport at $T > 0$ was the Hubbard chain with one particle $N_{\uparrow} = 1$ in a bath of fermions corresponding to $N_{\downarrow} \sim L/2$ [2,16].

As in the XXZ spin chain, in the Hubbard model at $U > 0$ there might persist finite dc contributions $\tilde{\sigma}_c(\omega \to 0) > 0$, $\tilde{\sigma}_s(\omega \to 0) > 0$ [13] besides the ballistic components at general $\bar{n} \neq 1, \bar{m} \neq 0$. On the other hand, the evolution with $U > 0$ is expected to be more generic since, unlike the XXZ chain, there are no anomalies associated with particular U values. We numerically investigate here only the case of charge conductivity $\tilde{\sigma}_c(\omega)$ at quarter-filling $\bar{n} = 1/2$ and $\bar{m} = 0$. In Fig. 7 we present results obtained on the chain of $L = 20$ sites via MCLM, presented in Fig. 7(a) as a scan through the range of small/modest $0 < U/t \leqslant 2$ and in Fig. 7(b) for selected modest/large $U/t = 1, 2, 4, 8$. It should be first mentioned that quite similar results emerge when performing ED for $L = 16$, hence the L dependence appears to be weak, at least in the accessible L range.

Apart from the dissipationless component, which in the presented quarter-filling case takes approximately half of the sum rule [29], the variation for small/modest $U/t > 0$ is quite analogous to the $\Delta \gtrsim 0$ in the XXZ spin chain. For $U/t \leqslant 1.5$ the spectra $\tilde{\sigma}_{reg}(\omega)$ are dominated by a single peak at $\omega_p \propto U$ with a vanishing dc limit $\tilde{\sigma}^0_{reg} \to 0$. For larger $U/t > 1.5$ the structure in Fig. 4 develops more components: (a) large-ω contribution which directly reflects the scale $\omega \sim U$, and (b) the remaining low-ω structure apparently still reveals two not well separated peaks, where the lower one remains at $\omega_{p1} \sim t/2$ and the upper broader one $\omega \lesssim 3t/2$ is related to the incoherent bandwidth. Most important for the present study, presented results suggest vanishing $\tilde{\sigma}_{reg}(\omega \to 0)$ or at least allow only for a very small upper bound of $\tilde{\sigma}^0_{c,reg}$.

IV. CONCLUSIONS

In this paper we presented the numerical results for dynamical transport response, i.e., high-temperature $T \to \infty$
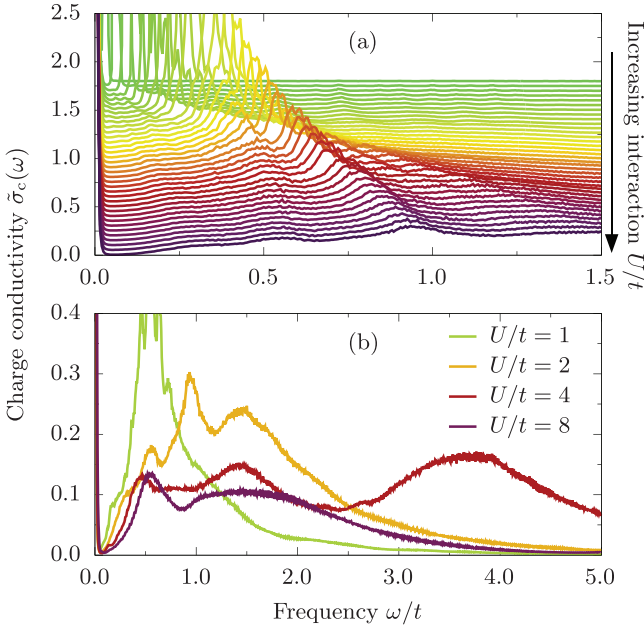
FIG. 7. (a) Charge conductivity $\tilde{\sigma}_c(\omega)$ for the 1D Hubbard model at quarter-filling $\bar{n} = 1/2$ and zero magnetization $\bar{m} = 0$, obtained via MCLM for a chain of $L = 20$ sites and $M_L = 5 \times 10^3$ steps. (a) The scan for the whole interaction $0 < U/t < 2$ range. (b) Spectra for selected moderate/large $U/t = 1, 2, 4, 8$.

conductivities $\sigma(\omega)$, in two integrable lattice 1D models, i.e., the anisotropic Heisenberg XXZ model and the Hubbard model. Since our aim was to resolve the low-ω behavior in terms of dissipationless $\mathcal{D}$ component and the potential remnant diffusive contribution $\sigma_{\text{reg}}(\omega \to 0)$, we adapted the MCLM approach by allowing for large systems (up to $L = 32$ for the XXZ and $L = 20$ for the Hubbard model), as well as high frequency resolution $\delta\omega/(J, t) \sim 10^{-3}$. Our results can be summarized as:

(a) Concerning the comparison with previous numerical results (nearly exclusively) on the XXZ chain, we are in agreement with DQT results for the stiffness $\mathcal{D}(\Delta) = I(\omega \to 0)/2$ obtained for system sizes $L \leqslant 30$ with PBC [23,24]. Apparently we also agree with the results of tDMRG method [25,26] obtained for larger systems $L \leqslant 200$, e.g., presented for $\Delta = 0.5$ in Fig. 3(b). Since the latter time-dependent correlations are followed only up to times $\tau J \sim 35$, one cannot uniquely extract results for $\omega/J < 0.15$ [25], which is the essential range for the understanding of dynamics in the metallic $\Delta < 1$ regime.

(b) Besides a well established ballistic $\mathcal{D} > 0$ contribution, a regular part of dynamical spectra $\tilde{\sigma}(\omega)$ are quite complex in the XXZ model, revealing a several-peak structure at general $\Delta \neq \Delta_m$. The most controlled regime appears to be that of small $\Delta \ll 0.5$, where both ED and MCLM calculations at finite Δ confirm a single-peak structure of $\tilde{\sigma}(\omega)$ with the position at $\omega_p \propto \Delta$ and fast exponential-like decay for $\omega > \omega_p$. The latter is also consistent with the calculation within the DPT method for $\Delta \to 0$, performed here exactly up to system sizes of $L = 28$. Our results reveal $\tilde{\sigma}_{\text{reg}}(\omega < \omega_p) \propto \omega^b$ with $1 \leqslant b \leqslant 2$ and $\omega_p > 0$ for $L \to \infty$, i.e., the absence of a diffusive contribution and a qualitative agreement with

the argument following from the level-crossing scenario [30]. However, finite-size effects are still substantial so it is hard to exclude that $\omega_p = 0$ for $L \to \infty$.

(c) Quite informative are the results for commensurate $\Delta = \Delta_m$, in particular for $\Delta_3 = 1/2$ and somewhat less for $\Delta_4 = 1/\sqrt{2}$, where Fig. 3 does not leave much room for dc diffusion $\tilde{\sigma}_{\text{reg}}^0 > 0$ in our finite-size systems, although the observed finite-size gap ω_g reveals some L dependence, so that we cannot exclude its closing for $L \to \infty$ and possible agreement with the GHD results for $\tilde{\sigma}_{\text{reg}}^0$ [33,36].

(d) The spectral evolution is most difficult to follow in the vicinity of commensurate anisotropy $\Delta \sim \Delta_m$, which becomes very involved in the regime $\Delta > 0.5$. Namely, each Δ_m appears to be a source for additional structure appearing as the peak at $\omega_{pm} \propto |\Delta - \Delta_{m+1}|$. Such development can be, e.g., directly followed via ED and MCLM for $m = 2$ and $m = 4$, emerging from the lifting of additional large (exponentially increasing with L) degeneracies at Δ_m (see Figs. 1 and 5). Less conclusive is the case of $\Delta_3 = 0.5$, where large-L results still reveal such peaks, but considered PBC systems with $L = 4\mathcal{L}$ do not seem to exhibit explicitly such degeneracies. In any case, such a scenario should effectively reappear with increasing L, as we also confirm by comparing in Fig. 1 results for systems with $L = 20$ and $L = 32$.

(e) It should be remarked that the emerging spectral components for $\Delta \neq \Delta_m$ are also the origin for the GHD expectation concerning a singular $\tilde{\sigma}_{\text{reg}}(\omega) \propto \omega^{-\alpha}$ with $\alpha > 0$ [36] in the vicinity of commensurate Δ_m. To justify the latter, besides the jump of $\mathcal{D}$ and of the remaining sum rule $\tilde{\sigma}_{\text{reg}}(\omega)$, an additional assumption is a power-law decay in time of current correlation $\langle j(\tau)j \rangle - \langle j(\infty)j \rangle$. However, our finite-$L$ results for $\tilde{\sigma}_{\text{reg}}(\omega)$ are compatible with an oscillating time evolution to final $\langle j(\tau \to \infty)j \rangle \propto \mathcal{D} > 0$ value, which is visible also in the tDMRG results in [25].

(f) The evolution within the 1D Hubbard model appears somewhat simpler when considering, e.g., the regular part of the high-T charge conductivity $\tilde{\sigma}_{c,\text{reg}}(\omega)$ in the ballistic regime away from half-filling $\bar{n} = 1$. For the particular case of quarter-filling and zero magnetization ($\bar{n} = 1/2$, $\bar{m} = 0$), our results reveal a single-peak structure for modest $U/t < 1$ with the peak $\omega_p \propto U$ and vanishing $\tilde{\sigma}_{c,\text{reg}}^0$, quite in analogy with the $\Delta \to 0$ in the XXZ chain. For larger $U/t > 1$, a large-ω peak splits off with $\omega_p \sim U$ while $\omega < 2t$ regime still reveals some nontrivial two-peak structure, but again apparently with no diffusive contribution at low-ω. The latter is consistent with previous results for a particular case of the 1D Hubbard model, i.e., representing a single particle in a fermionic bath [16].

(g) The arguments and predictions for the possible coexistence of ballistic and diffusive transport emerge within the GHD approach, which directly implies the limit $L \to \infty$. Since we hardly see clear evidence for $\tilde{\sigma}_{\text{reg}}^0 > 0$, even in largest systems ($L = 32$), a minimum conclusion could be that such a diffusion is anomalous, i.e., is not reflected in a physically relevant mean free path $\lambda < L$. Such a case is not excluded and can emerge also in integrable quantum lattice systems. A closely related example is the high-T diffusion in the easy-axis XXZ model at $\Delta \geqslant 1$, where $\mathcal{D} = 0$ and apparent $\tilde{\sigma}_{\text{reg}}^0 > 0$ implies an effective $\lambda_{\text{eff}} \sim 1$, whereas $\tilde{\sigma}(\omega)$ still exhibits anomalous $\omega \propto 1/L$ finite-size

effects [1,41,47]. In fact, we can confirm such anomalous L dependence in our analysis on approaching $\Delta \to 1$, where we confirm the superdiffusive dynamical scaling $\tilde{\sigma}(\omega) \propto \omega^{-1/3}$ [34,36,37,42,44]. Such quite explicit L dependence signals the importance of the relevant order of limits $L \to \infty$ and $t \to \infty$ (or $\omega \to 0$). Namely, different quantities can require different limits, and in particular σ_{reg}^0 (evaluated at $L \to \infty$ first) might not correspond to energy dissipation (heating) inside the system, as found, e.g., for the easy-axis side $\Delta > 1$ [48], i.e., the diffusion (as, e.g., evaluated within GHD) might be dissipationless.

(h) Finally, it should be reminded that even a weak integrability-breaking perturbation (e.g., a single impurity in the XXZ chain [49]) in the finite MB system with PBC turns,

e.g., the singular $\sigma(\omega)$ response into a Lorentzian-type normal diffusion with a well defined characteristic λ.

[1] B. Bertini, F. Heidrich-Meisner, C. Karrasch, T. Prosen, R. Steinigeweg, and M. Žnidarič, Finite-temperature transport in one-dimensional quantum lattice models, Rev. Mod. Phys. **93**, 025003 (2021).

[2] H. Castella, X. Zotos, and P. Prelovšek, Integrability and Ideal Conductance at Finite Temperatures, Phys. Rev. Lett. **74**, 972 (1995).

[3] X. Zotos, Finite Temperature Drude Weight of the One-Dimensional Spin-1/2 Heisenberg Model, Phys. Rev. Lett. **82**, 1764 (1999).

[4] J. Benz, T. Fukui, A. Klümper, and C. Scheeren, On the finite temperature Drude weight of the anisotropic Heisenberg chain, J. Phys. Soc. Jpn. **74**, 181 (2005).

[5] A. Pavlis and X. Zotos, Dressed excitations, thermodynamics and relaxation in the XXZ Heisenberg model, J. Stat. Mech.: Theory Exp. (2020) 013101.

[6] A. Urichuk, J. Sirker, and A. Klümper, Analytical results for the low-temperature Drude weight of the XXZ spin chain, Phys. Rev. B **103**, 245108 (2021).

[7] X. Zotos, F. Naef, and P. Prelovsek, Transport and conservation laws, Phys. Rev. B **55**, 11029 (1997).

[8] T. Prosen, Open XXZ Spin Chain: Nonequilibrium Steady State and a Strict Bound on Ballistic Transport, Phys. Rev. Lett. **106**, 217206 (2011).

[9] T. Prosen and E. Ilievski, Families of Quasilocal Conservation Laws and Quantum Spin Transport, Phys. Rev. Lett. **111**, 057203 (2013).

[10] T. Prosen, Quasilocal conservation laws in XXZ spin-1/2 chains: Open, periodic and twisted boundary conditions, Nucl. Phys. B **886**, 1177 (2014).

[11] R. G. Pereira, V. Pasquier, J. Sirker, and I. Affleck, Exactly conserved quasilocal operators for the XXZ spin chain, J. Stat. Mech. (2014) P09037.

[12] E. Ilievski and J. De Nardis, Microscopic Origin of Ideal Conductivity in Integrable Quantum Models, Phys. Rev. Lett. **119**, 020602 (2017).

[13] E. Ilievski and J. De Nardis, Ballistic transport in the one-dimensional Hubbard model: The hydrodynamic approach, Phys. Rev. B **96**, 081118(R) (2017).

[14] V. B. Bulchandani, R. Vasseur, C. Karrasch, and J. E. Moore, Bethe-Boltzmann hydrodynamics and spin transport in the XXZ chain, Phys. Rev. B **97**, 045407 (2018).

[15] X. Zotos and P. Prelovšek, Evidence for ideal insulating or conducting state in a one-dimensional integrable system, Phys. Rev. B **53**, 983 (1996).

[16] H. Castella and X. Zotos, Finite-temperature mobility of a particle coupled to a fermionic environment, Phys. Rev. B **54**, 4375 (1996).

[17] F. Naef and X. Zotos, Spin and energy correlations in the one dimensional spin-1/2 Heisenberg model, J. Phys.: Condens. Matter **10**, L183 (1998).

[18] F. Heidrich-Meisner, A. Honecker, D. C. Cabra, and W. Brenig, Zero-frequency transport properties of one-dimensional spin-$\frac{1}{2}$ systems, Phys. Rev. B **68**, 134436 (2003).

[19] F. Heidrich-Meisner, A. Honecker, and W. Brenig, Transport in quasi one-dimensional spin-1/2 systems, Eur. Phys. J.: Spec. Top. **151**, 135 (2007).

[20] M. Rigol and B. S. Shastry, Drude weight in systems with open boundary conditions, Phys. Rev. B **77**, 161101(R) (2008).

[21] M. Žnidarič, Spin Transport in a One-Dimensional Anisotropic Heisenberg Model, Phys. Rev. Lett. **106**, 220601 (2011).

[22] J. Herbrych, P. Prelovšek, and X. Zotos, Finite-temperature Drude weight within the anisotropic Heisenberg chain, Phys. Rev. B **84**, 155125 (2011).

[23] R. Steinigeweg, J. Gemmer, and W. Brenig, Spin-Current Autocorrelations from Single Pure-State Propagation, Phys. Rev. Lett. **112**, 120601 (2014).

[24] R. Steinigeweg, J. Gemmer, and W. Brenig, Spin and energy currents in integrable and nonintegrable spin-$\frac{1}{2}$ chains: A typicality approach to real-time autocorrelations, Phys. Rev. B **91**, 104404 (2015).

[25] C. Karrasch, D. M. Kennes, and F. Heidrich-Meisner, Spin and thermal conductivity of quantum spin chains and ladders, Phys. Rev. B **91**, 115130 (2015).

[26] C. Karrasch, Hubbard-to-Heisenberg crossover (and efficient computation) of Drude weights at low temperatures, New J. Phys. **19**, 033027 (2017).

[27] M. Ljubotina, M. Žnidari, and T. Prosen, Spin diffusion from an inhomogeneous quench in an integrable system, Nat. Commun. **8**, 16117 (2017).

[28] R. J. Sánchez and V. K. Varma, Finite-size anomalies of the Drude weight: Role of symmetries and ensembles, Phys. Rev. B **96**, 245117 (2017).

[29] M. Mierzejewski, J. Herbrych, and P. Prelovšek, Ballistic transport in integrable quantum lattice models with degenerate spectra, Phys. Rev. B **103**, 235115 (2021).

[30] J. Herbrych, R. Steinigeweg, and P. Prelovšek, Spin hydrodynamics in the $s = \frac{1}{2}$ anisotropic Heisenberg chain, Phys. Rev. B **86**, 115106 (2012).

[31] J. Sirker, R. G. Pereira, and I. Affleck, Diffusion and Ballistic Transport in One-Dimensional Quantum Systems, Phys. Rev. Lett. **103**, 216602 (2009).

[32] J. Sirker, R. G. Pereira, and I. Affleck, Conservation laws, integrability, and transport in one-dimensional quantum systems, Phys. Rev. B **83**, 035115 (2011).

[33] J. De Nardis, D. Bernard, and B. Doyon, Hydrodynamic Diffusion in Integrable Systems, Phys. Rev. Lett. **121**, 160603 (2018).

[34] E. Ilievski, J. De Nardis, M. Medenjak, and T. Prosen, Superdiffusion in One-Dimensional Quantum Lattice Models, Phys. Rev. Lett. **121**, 230602 (2018).

[35] S. Gopalakrishnan, D. A. Huse, V. Khemani, and R. Vasseur, Hydrodynamics of operator spreading and quasiparticle diffusion in interacting integrable systems, Phys. Rev. B **98**, 220303(R) (2018).

[36] U. Agrawal, S. Gopalakrishnan, R. Vasseur, and B. Ware, Anomalous low-frequency conductivity in easy-plane XXZ spin chains, Phys. Rev. B **101**, 224415 (2020).

[37] V. B. Bulchandani, S. Gopalakrishnan, and E. Ilievski, Superdiffusion in spin chains, J. Stat. Mech. (2021) 084001.

[38] M. W. Long, P. Prelovšek, S. El Shawish, J. Karadamoglou, and X. Zotos, Finite-temperature dynamical correlations using the microcanonical ensemble and the Lanczos algorithm, Phys. Rev. B **68**, 235106 (2003).

[39] P. Prelovšek and J. Bonča, Ground state and finite temperature Lanczos methods, in *Strongly Correlated Systems - Numerical Methods*, edited by A. Avella and F. Mancini (Springer, Berlin, 2013).

[40] P. Prelovšek, M. Mierzejewski, O. Barišić, and J. Herbrych, Density correlations and transport in models of many-body localization, Ann. Phys. (Berl.) **529**, 1600362 (2017).

[41] P. Prelovšek, S. El Shawish, X. Zotos, and M. Long, Anomalous scaling of conductivity in integrable fermion systems, Phys. Rev. B **70**, 205129 (2004).

[42] M. Ljubotina, M. Žnidarič, and T. Prosen, Kardar-Parisi-Zhang Physics in the Quantum Heisenberg Magnet, Phys. Rev. Lett. **122**, 210602 (2019).

[43] S. Gopalakrishnan and R. Vasseur, Kinetic Theory of Spin Diffusion and Superdiffusion in XXZ Spin Chains, Phys. Rev. Lett. **122**, 127202 (2019).

[44] J. De Nardis, M. Medenjak, C. Karrasch, and E. Ilievski, Anomalous Spin Diffusion in One-Dimensional Antiferromagnets, Phys. Rev. Lett. **123**, 186601 (2019).

[45] J. De Nardis, S. Gopalakrishnan, R. Vasseur, and B. Ware, Stability of Superdiffusion in Nearly Integrable Spin Chains, Phys. Rev. Lett. **127**, 057201 (2021).

[46] L. Zadnik, M. Medenjak, and T. Prosen, Quasilocal conservation laws from semicyclic irreducible representations of Uq(sl2) in XXZ spin-1/2 chains, Nucl. Phys. B **902**, 339 (2016).

[47] R. Steinigeweg, J. Herbrych, P. Prelovšek, and M. Mierzejewski, Coexistence of anomalous and normal diffusion in integrable Mott insulators, Phys. Rev. B **85**, 214409 (2012).

[48] M. Mierzejewski, J. Bonča, and P. Prelovšek, Integrable Mott Insulators Driven by a Finite Electric Field, Phys. Rev. Lett. **107**, 126601 (2011).

[49] O. S. Barišić, P. Prelovšek, A. Metavitsiadis, and X. Zotos, Incoherent transport induced by a single static impurity in a Heisenberg chain, Phys. Rev. B **80**, 125118 (2009).